International Journal on Interactive Design and Manufacturing (IJIDeM)
https://doi.org/10.1007/s12008-023-01248-1

ORIGINAL PAPER

3D scanning of Upper Limb anatomy by a depth-camera-based system

Paolo Neri[1] · **Alessandro Paoli**[1] · **Beatrice Aruanno**[1] · **Sandro Barone**[1] · **Francesco Tamburrino**[1] · **Armando V. Razionale**[1]

Received: 25 July 2022 / Accepted: 14 February 2023

Abstract
The 3D reconstruction of upper limb anatomy plays a significant role in many biomedical fields such as ergonomics, motion rehabilitation, and prosthesis design. In the last few years, the technical advancement of consumer-grade depth cameras has supported the development of portable and low-cost optical 3D body scanners for healthcare applications. The real-time scanning of human body parts, however, still represents a complex task due to the non-stationary nature of the scanning target. This issue imposes that the scanning time must be reduced as much as possible to minimize scanning artifacts. In this regard, depth cameras can capture geometrical information at video frame rates, thus guaranteeing fast acquisition times. Furthermore, the simultaneous use of multiple sensors would minimize undercut geometries, which impair the 3D reconstruction's completeness. In this work, a portable 3D optical scanner has been developed by rigidly assembling three Intel® RealSense™ D415 depth cameras on a lightweight circular frame. The three sensors are mutually calibrated, by using a 3D printed calibration specimen, to simultaneously align acquisitions from the three different camera viewpoints for each scanner pose. The system's effectiveness has been assessed by acquiring the geometry of both a plaster hand and a human hand and comparing the results with those obtained by a high-end stationary structured light scanner. The developed system represents a low-cost handheld alternative to existing body scanners for collecting and storing 3D anatomical data, which can be used in the design process of bespoke medical devices.

Keywords 3D optical scanning · Upper Limb Reconstruction · Depth-camera · D415 Intel® RealSense™

1 Introduction and background

Non-contact 3D scanning of human body anatomy has shown, in the last decade, to have a strong impact on many fields such as healthcare [1], sports [2], ergonomics [3], fashion and apparel [4], clothing [5], and entertainment industry [6]. In particular, the use of optical 3D scanning technologies has opened new possibilities for obtaining patient-specific geometry with minimally invasive procedures, low effort, and good accuracy. Nowadays, the use of optical 3D scanners is recognized as a trending process to support the design of bespoke devices and customized rehabilitation approaches that allow more effective and comfortable therapies [7–11]. For instance, the rehabilitation of upper limb mobility, impaired by musculoskeletal disorders, greatly benefits from the creation of an advanced patient's biomechanical profile, whose starting point is the 3D scanning of the patient's upper limb anatomy. The conventional approach to acquire body sizes and patient's morphology is based on manual tape measurements, taken by medical practitioners, and plaster molds, respectively. Hand-crafting processes are then adopted to customize the medical device and enhance comfort once the patient wears the prototype. However, these approaches are invasive, time-consuming, and often affected by a significant level of subjectivity. Also, this manufacturing practice cannot incorporate functional and design rules into the definition of the appliance shape. For these reasons, the standard procedure has been progressively replaced by computer-aided design (CAD) and computer-aided engineering (CAE) tools combined with Additive Manufacturing (AM) technologies, that allow the direct fabrication of fully functional parts starting from a 3D model, without involving the traditional manufacturing

✉ Paolo Neri
paolo.neri@unipi.it

[1] Department of Civil and Industrial Engineering, Mechanical Division, University of Pisa, Largo L. Lazzarino 1, 56122 Pisa, Italy

Published online: 26 February 2023

processes [7, 9, 12, 13]. In this regard, optical 3D scanning offers many advantages in terms of non-invasiveness, ease of use, and low cost, making it appealing to reconstruct, measure and track evolutions of human anatomy for a variety of clinical applications. Many technologies exist, and countless are the scientific community's approaches to generate detailed 3D models, including color and texture, at very fast rates [14]. The recent technological advancement in off-the-shelf depth cameras (RGB-D cameras) has further pushed toward the definition of low-end portable devices suitable also for small clinical centers, thus consolidating the 3D optical reconstruction of human body parts within biomedical applications [8, 15–19]. 3D scanning of the human upper limbs (i.e., hands, fingers, wrists, and forearms) is not a straightforward task as the patient should keep the arm in the same position for the whole duration of the measurement process. For this reason, real-time single-shot scanning techniques outperform the popular phase shift-based structured light methods in the minimization of artifacts due to involuntary movements [20]. However, critical issues remain since the fingers have many degrees of freedom and can undergo small involuntary tremors. Furthermore, the hand and fingers shape lead to self-occlusions, which reduce the 3D scanned data completeness.

In the present work, a compact and low-cost 3D scanning system, composed of multiple RGB-D sensors, has been developed to perform real-time acquisitions of upper limb anatomy. A similar approach was developed in [17] and [8] by arranging four and eight Intel® RealSense™ SR300 depth cameras, respectively, on 720 mm diameter circular rings, fixed on a desk. The two different architectures, which mainly differ in the field of view, were defined to acquire hand–wrist–arm anatomy all at once. However, the SR300 module is based on the sequential projection of fringe patterns and the simultaneous use of multiple devices is subjected to interference problems if different cameras partly share the same field of view. For this reason, the overall acquisition must be carried out by turning on the laser intensity of the projector of each individual sensor in sequence. This process leads to an overall acquisition time of 1.2 s, even if the SR300 Intel® RealSense™ works up to 60 fps. Moreover, these configurations define static architectures, which may limit their use for patients suffering from partially inhibited musculoskeletal system function (i.e., dystonia disorders).

In the present paper, three D415 Intel® RealSense™ depth cameras have been assembled on a circular frame to define a lightweight handheld scanner. The depth cameras arrangement has been defined as a tradeoff between the hardware complexity and cost (i.e., number of cameras) and the minimization of undercuts of the acquired geometry. The developed hand-held configuration is oriented at obtaining a compact and lightweight design which can be used also outside clinical centres (i.e., patient's home). The configuration has been also conceived to scan patients affected by hyperkinetic movement disorders that are not able to maintain the arm in a stable condition. An ad-hoc and fully automatic calibration procedure has been also developed to find the relative placement between the cameras, thus allowing to automatically align, in the same reference frame, the point clouds captured by the three independent sensors during the scanning stage. The system's effectiveness has been assessed by acquiring the geometry of both plaster and a human hand and comparing the obtained results with those obtained by using a high-end stationary structured light scanner.

2 Hardware set-up

The 3D scanning of human body anatomy presents peculiar challenges related to undercuts, which requires different scans from multiple viewpoints to obtain a complete reconstruction of the target surface. The main issue in this scenario consists in the possibility for the patient to stay still throughout the whole acquisition process, to avoid any artifact in the final scanning results. As a result, the scanning device must allow for fast and robust acquisitions, and the scanning protocol, which follows suggestions given by clinicians, should be completed in the range of 60 s to avoid overtiredness in the patient who is forced to hold the arm steady for an extended period. For this reason, a specific 3D scanner was developed by combining three independent D415 Intel® RealSense™ depth cameras, which are fast (up to 90 fps), high resolution (up to 1280×720 pixels), and low-cost 3D scanning devices [21]. A full metrological characterization of the depth camera was presented in [22], demonstrating its suitability for biomedical purposes. The integration of three distinct sensors allows widening the field of view of each single acquisition, thus reducing the overall number of frames required to obtain a full 3D reconstruction. Figure 1 shows the defined layout, with the three sensors mounted on a ring. Figure 1(a) presents the schematic top and lateral views of the architecture, highlighting its main dimensions and the positioning of the three sensors along the circumference hoop and their orientation with respect to radial and axial directions. This configuration allows for two different forearm positions during the scanning process: in front of the circular frame and inside the ring itself. These two scenarios were conceived to improve the scanner's usability, considering that not all patients are able to keep their arms extended (e.g., patients affected by dystonia disorders). The sensor placement was optimized to achieve a twofold result. Firstly, the opposed sensors obtain a wide angle around the arm, so that a large

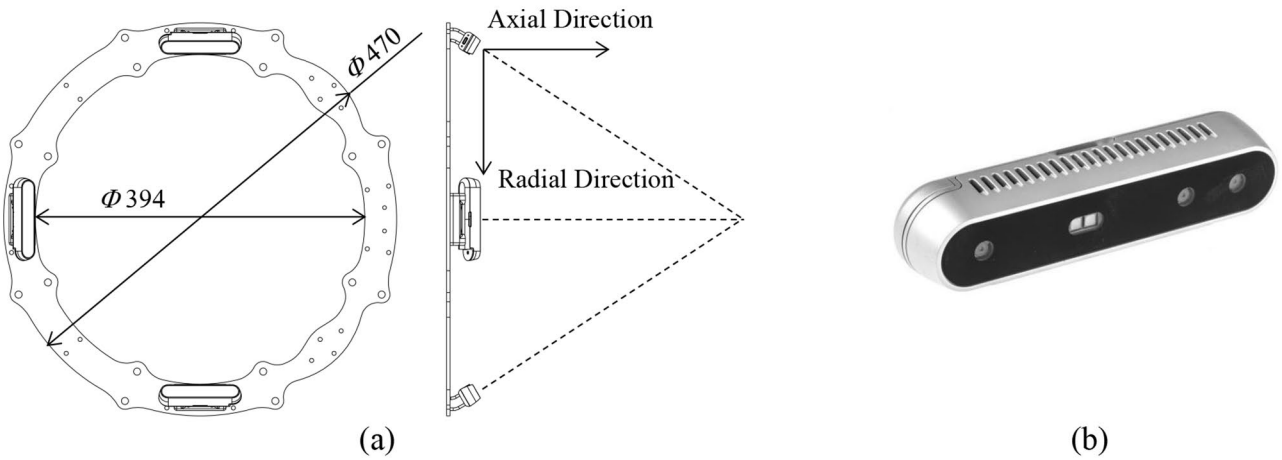

Fig. 1 Overview of the developed scanner: (a) schematic views and (b) D415 Intel® RealSense™ depth camera

Fig. 2 Final prototype of the scanning device: (a) system's overview and (b) detailed view of the sensor cover

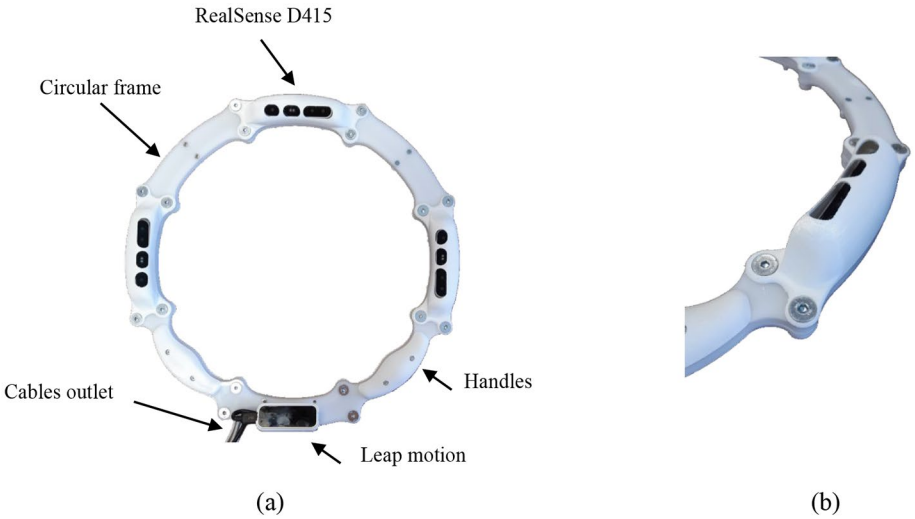

field of view is acquired for each frame. Secondly, the last sensor is oriented to acquire the typical arm undercut, which is generally represented by the back surface of the thumb. This layout results in a versatile, lightweight, and handheld device, which can be adapted to specific patient clinical conditions, even in the case of severe musculoskeletal disorders and reduced mobility of the impaired limb. It is worth noting that the D415 Intel® RealSense™ camera is based on an active infrared stereo depth technology. The sensor is equipped with a color camera, two infrared cameras, and an infrared projector (Fig. 1(b)). The projector projects a static pattern, which is used to increase the texture of low-textured scenes. The use of a static pattern instead of a structured light approach (i.e., sequential projection of fringe patterns as for the SR300 Intel® RealSense™ depth camera) avoids interference problems between the different sensors, which can simultaneously acquire the target surface.

Since the device is designed to be used also by non-expert users (i.e., medical teams) and in combination with actual patients, a design effort was spent to obtain a prototype that was usable, robust, and comfortable for both the patients and the users. To this extent, the mechanical structure of the ring was designed in three layers of Polymethylmethacrylate. The top and bottom layers are used as interfaces for both sensors and handles, while the middle layer is designed to contain the cables (Fig. 2). All the cables pass through the top layer and are routed in the middle layer to the outlet. Each sensor is housed within a 3D printed cover, to protect the devices from accidental impacts and optics from staining. The final prototype has an external diameter of 470 mm and a weight of 1520 g.

Figure 2 also shows an Ultraleap LeapMotion controller [23] assembled on the circular frame of the scanning device. This sensor is an optical hand tracking device that combines two infrared cameras and LEDs to generate a virtual skeletal

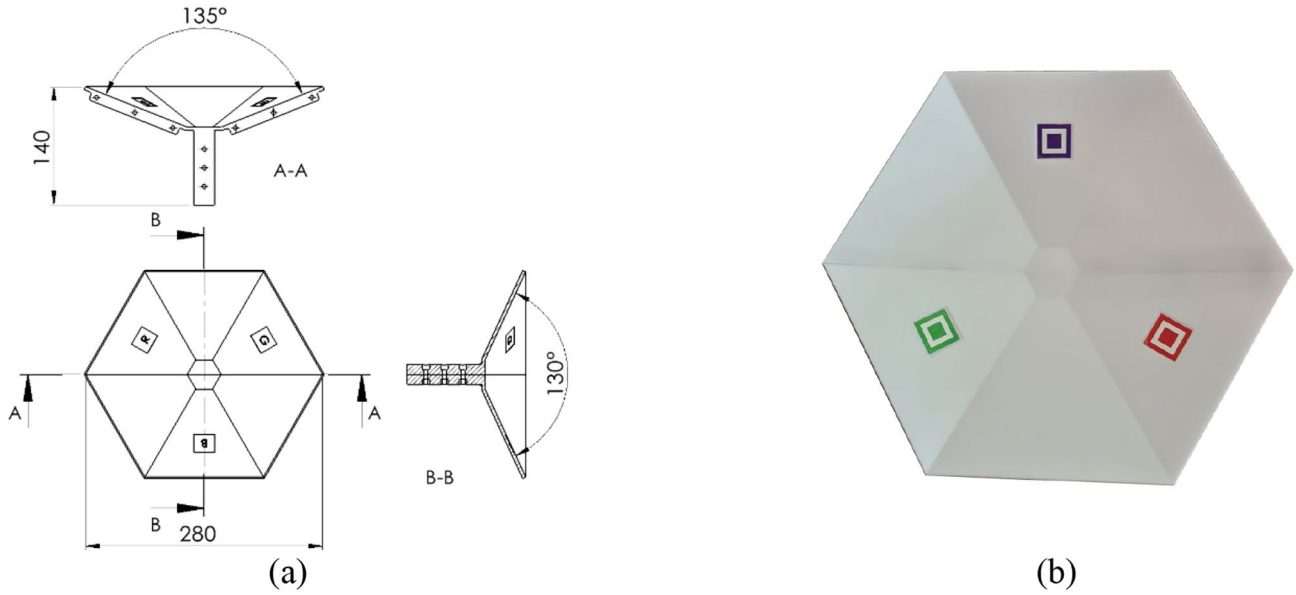

Fig. 3 Calibration specimen: (a) geometry, (b) view of the upper planar surfaces with colored markers

model of the hands based on the positions and rotations of the joints. It was added to the frame in order to assess the patient's hand range of motion, which, however, is outside the aim of this work. Finally, the equipment is completed by a pedal switch (not shown in Fig. 2). The switch allows for the one-person operation of the scanner. The user, by acting on the pedal, can autonomously save the frames even while holding the scanner with both hands.

2.1 Calibration

The acquisition of multiple frames from different viewpoints requires the alignment of the point clouds to a common reference frame. This task is accomplished by an extrinsic calibration procedure, which is possible since the three sensors are rigidly connected to the same structure. The calibration allows determining the roto-translation matrices that geometrically refer each sensor to the others. This is achieved through a coarse-to-fine approach [24] that uses three markers to evaluate the first initial value of the extrinsic parameters and then refines these values using an iterative closest point (ICP) algorithm that minimizes the distances between overlapping areas of the point clouds acquired by the three sensors. To this extent, a specific calibration specimen (Fig. 3) was designed and 3D printed with PLA (polylactic acid) material by a FFF (fused filament fabrication) machine. The specimen was made in two distinct parts, assembled through bolt connections, to take into account the limited sizes of the printing volume. The specimen has wide planar surfaces, which provide a great number of measurement points for the registration process. The calibration problem would have been under-constrained if only a planar surface had been used. Thus, a 135° angle was set between two diametrically opposite faces of the specimen (Fig. 3(a)). The value of the angle was chosen to be smaller than 180°, but it was limited by visibility issues: indeed, the aim was that all the faces were visible by all the three sensors in each acquisition. Additionally, three colored markers are glued to the specimen surface (Fig. 3(b)). These markers can be automatically detected by elaborating the RGB images which are captured by the Intel® RealSense™ sensors.

The factory calibration of the sensors can be exploited to reproject the centers of the markers on the 3D point cloud, thus obtaining three key points for each sensor's acquisition. Figure 4(a), (b), and (c) show an example of the point clouds, along with the colored marker location, acquired by the three sensors for a scanner pose. The different colors are used to automatically code each marker and the key points triplets are used to obtain a first rough alignment of the point clouds. The result of this step is shown in Fig. 4(d), which evidences that the acquired geometries, even if correctly aligned, are not perfectly overlapped. Indeed, in Fig. 4(d) one specific color is dominant in different areas of the registered clouds, meaning that one of the three clouds is in front of the others, and not precisely overlapped. This is due to marker detection inaccuracies, which may be ascribed to different lighting conditions and center detection errors. For this reason, the alignment is refined by an ICP algorithm, which exploits the overlapping regions of the three-point clouds to obtain an accurate registration. The result of this refinement step is shown in Fig. 4(e), which highlights a

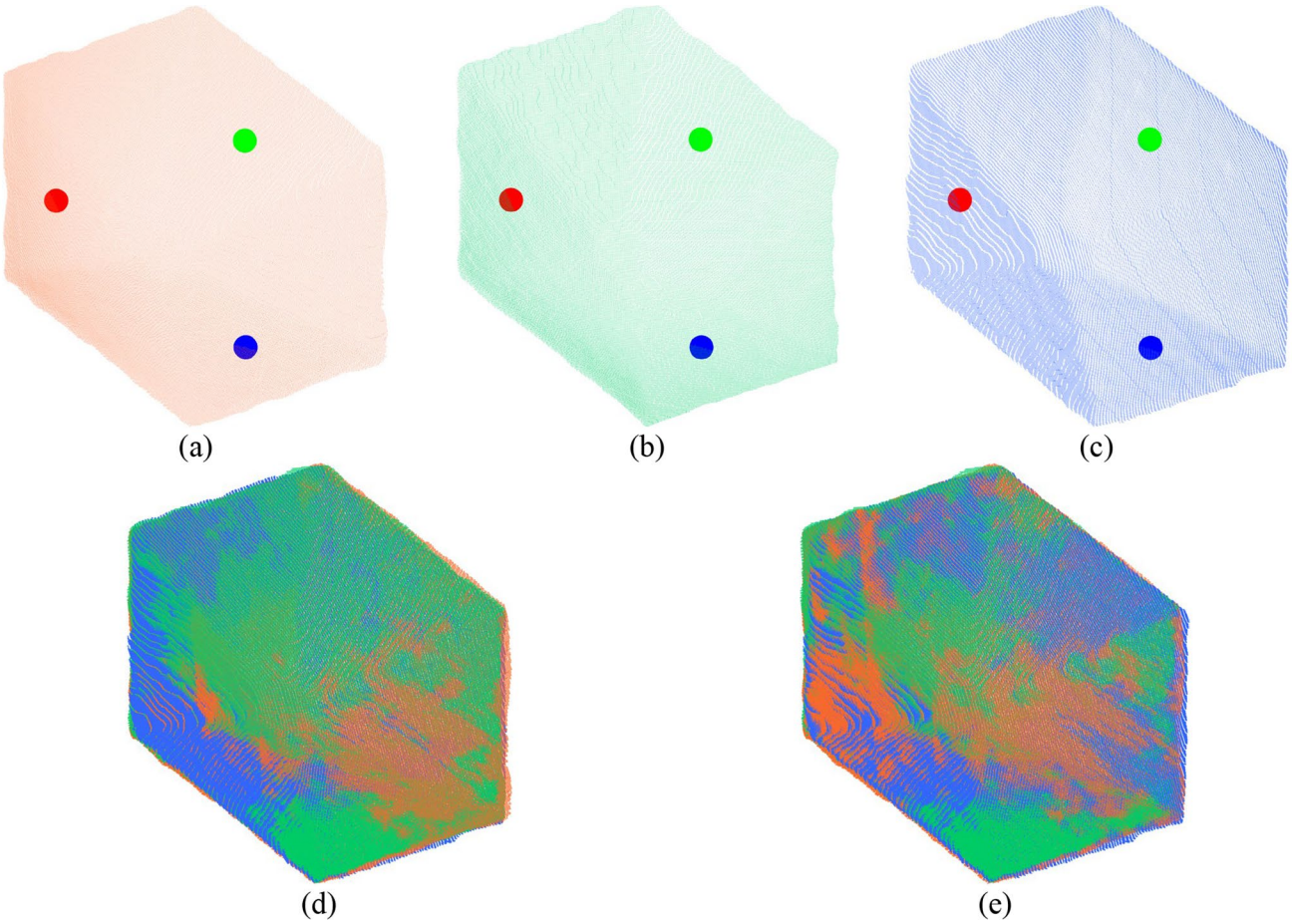

Fig. 4 Point clouds acquired by the three sensors and used for the calibration process: (a) first sensor, (b) second sensor, (c) third sensor, (d) rough alignment based on automatic markers detection, and (e) final registration based on the ICP algorithm

Table 1 Performance of the calibration procedure during manual scanning

	1Vs2 (mm)			1Vs3 (mm)			2Vs3 (mm)		
	μ	|μ|	σ	μ	|μ|	σ	μ	|μ|	σ
Scan1	-0.16	1.08	1.47	-0.25	0.92	1.17	0.04	0.84	1.08
Scan2	-0.76	1.28	1.42	-0.14	1.20	1.43	0.70	1.43	1.63

better final overlapping of the scans: it is not possible to note regions were one single color is dominant, meaning that the overlapping of the clouds is improved and that points belonging to different clouds (and thus having different colors) are mixed after the use of the ICP algorithm. The overall roto-translation matrices that transform each point cloud from the sensor reference frame to the final common reference frame are stored in a calibration file, which is used during the patient's 3D scanning to align the three point clouds corresponding to a scanner pose.

Experimental tests have been carried out to evaluate the accuracy of the calibration data in the automatic alignment of point clouds deriving from the three sensors during actual scanning. The calibration specimen was fixed to a support, while the scanner was manually placed in front of the specimen. Four different acquisitions were performed, slightly varying the scanner pose with respect to the specimen in between acquisitions. Each of these four acquisitions is composed of the point clouds deriving from three sensors. Thus, for each acquisition, three comparison couples can be defined: cloud 1 vs. cloud 2, cloud 1 vs. cloud 3, and cloud 2 vs. cloud 3 (namely, 1Vs2, 1Vs3, and 2Vs3). It is then possible to compute the point-by-point deviation between the point clouds. The mean value (μ), the absolute mean value (|μ|), and the standard deviation value (σ) were then computed for each deviation vector (Table 1). Additionally, the

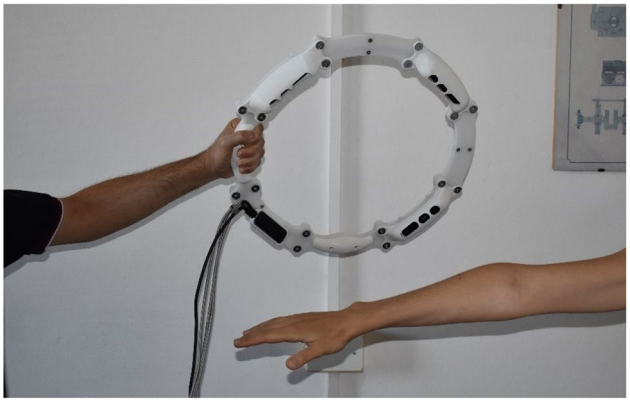

Fig. 5 Manual placement of the handheld scanner during acquisition: one-hand operation

same statistical measurements for the deviation vectors considered as a whole were computed to estimate the overall scanning trial accuracy ($\mu = -0.23$ mm, $|\mu| = 1.24$ mm, and $\sigma = 1.59$ mm). The developed optical scanner aims at acquiring human anatomical geometries. For this reason, the deviation values can be considered acceptable when compared with the measurement errors typical of 3D scanning of soft tissues, subject to involuntary movements.

2.2 Scanning workflow

The 360° scan of the patient's arm can be achieved by acquiring several consecutive frames of the limb. The described scanner can be held with one or two hands by the user (e.g., the therapist), and moved all around the patient arm in a circular path. Figure 5 shows an example of the scanner's manual positioning with respect to the patient's arm, during a one-hand operation. The widest field of view can be achieved by keeping aligned the scanner with the patient's arm. Several tests carried out by researchers and inexperienced therapists have shown that 6 to 10 views are sufficient to obtain a 360° reconstruction. The lower limit is generally obtained in the case of a fully stretched arm, while the upper limit is reached when the arm is in a folded position. The overall amount of time required to complete the scanning ranges between 30 and 50 s, depending on the total number of frames.

2.3 Point clouds elaboration

Data post-processing is a crucial step to convert the raw measurement data (i.e. list of 3D coordinates) to the 360° reconstruction of the upper limb. Even if the three acquisitions obtained for each scanner pose are aligned by exploiting calibration data, some small discrepancies can still exist, mainly due to the time delay between the acquisition of the three sensors. An automatic ICP algorithm is used on the three clouds to mitigate this phenomenon and further refine the registration results. Subsequently, point-cloud elaboration must be performed to remove outliers. An automatic algorithm was developed to detect point clusters in the clouds, providing a reference point-to-point distance that characterizes points belonging to the same cluster. It is assumed that smaller clusters are noisy outliers, while bigger clusters contain the relevant upper limb information. A threshold value was defined, based on the point numerosity of each cluster, which separates the arm data from the outliers, which are deleted. More aggressive processing can be achieved by augmenting the numerosity threshold value and reducing the point-to-point distance of the cluster, while less aggressive processing is obtained with smaller threshold values and larger cluster characteristic distance.

Denoised point clouds can then be aligned into a common reference frame, as exemplified in Fig. 6. The conventional pipeline for this task consists of a first rough alignment, which is generally obtained through the so-called 3-2-1 pairwise registration [25]. Adjacent point clouds are aligned by manually selecting at least three corresponding points on overlapping areas. The selection is generally driven by the presence of markers on the acquired object. Nevertheless, in this case, the procedure does not involve the application of the markers on the limb to reduce the preparation time and the measurement invasiveness for actual patients. Thus, the selection is carried out by looking at characteristic arm features, such as fingertips, elbow, wrist bones, or natural skin marks (Fig. 6(a)).

The rough alignment obtained by the 3-2-1 pairwise registration (Fig. 6(b)) can then be refined by an ICP algorithm, which exploits the overlapping region between adjacent point clouds to obtain a better registration result (Fig. 6(c)). After registering the clouds one by one, a final global registration process is done by applying the ICP algorithm to the whole dataset. The clouds elaboration step can be concluded by applying a conventional post-processing pipeline. Firstly, due to the overlapping of the clouds acquired from different viewpoints, uniform sampling is applied to avoid redundant data. Secondly, all the clouds can be merged into a unique data set, corresponding to the full arm geometry. Finally, a denoising algorithm can be applied to delete outliers and reduce surface roughness. The obtained data (i.e. 3D coordinates, RGB colors, and surface normals) can be stored as *ASCII* or *txt* files, or converted to surfaces and saved as *ply* or *step* files. Since the results of the post-processing procedure are not clearly visible at naked eye, Fig. 6(c) directly shows the final result (i.e., after ICP and post-processing pipeline) to avoid redundant pictures.

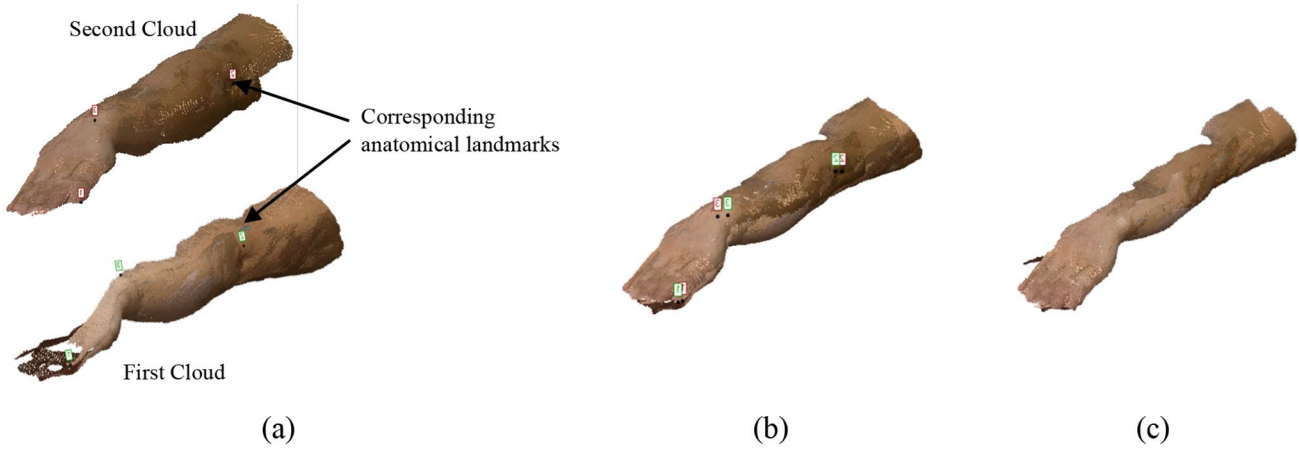

Fig. 6 Example of clouds alignment: (a) selection of corresponding key points, (b) rough registration, and (c) refined ICP registration

3 Assessment of scanner performance

Scanning results were compared with measurements obtained by using a high-end stationary structured light scanner to evaluate the performances of the developed system in two different situations. The first one consists in the 3D acquisition of a reference object consisting of a plaster human hand. This analysis is carried out by comparing both a single frame acquisition and the complete 360° acquisition of the target object by using the two scanners. This comparison provides an estimate of the accuracy of the developed device with respect to the stationary scanner, which is taken as a gold standard (at least in the case of stationary objects). The second one involves a single frame acquisition of a real human hand. This comparison aims to assess the performance of the scanner in a real situation, taking also into account the involuntary movements of a person during the acquisition process.

The stationary scanner (Fig. 7(a)) is composed of a DLP projector (resolution 1024×768 pixels) and a monochrome digital CCD camera (resolution 1280×960 pixels). The camera and projector are used as active devices of a stereo triangulation process. A calibration procedure is required to calculate the intrinsic and extrinsic parameters of the optical devices, with respect to an absolute reference system. The camera parameters are obtained by correlating the coordinates of known markers located on a calibration plate with the corresponding coordinates on the camera image plane. The projector is modeled like an inverse camera, exploiting its capability to generate both coded vertical and horizontal fringes [26]. The scanner accuracy has been tested for different working areas by measuring a reference nominal shape. In this work, the scanner has been arranged for a field of view of 280 mm × 210 mm, thus providing a lateral resolution of 0.28 mm and a measurement accuracy of 0.03 mm. Also, the scanning time for each pose is about 8 s.

3.1 Comparison with a plaster hand

Figure 7(a) shows the setup adopted for the acquisition of the plaster hand by the stationary scanner. The target object was placed on a desk with the dorsal side of the hand facing the scanner. Twelve different scans were taken by rotating the hand around its vertical axis of approximately 30° at a time. A manual alignment of adjacent scans by the 3-2-1 pairwise registration and a global refinement through the ICP algorithm was then carried out to obtain the final 3D model (Fig. 7(b)).

The acquisition of the plaster hand was repeated with the developed hand-held scanner. The hand was placed on a desk and a total number of 12 different frames were captured by manually positioning the scanner. After the acquisition and the registration procedure, described in the previous paragraph, the final mesh visible in Fig. 7(c) was obtained.

As can be noted, the high-end stationary scanner has a higher spatial resolution, which allows for a more detailed acquisition of the hand. Nevertheless, it is worth noting that this detail level is not necessarily required for the design of bespoke devices, since they must fit on soft tissues (patient's skin) that can be deformed in the order of some millimeters [1, 11, 27].

The first comparison to evaluate the scanner performance regards the full acquisition of the plaster hand. Figure 8 shows the 3D deviation maps and the deviation values histogram obtained by comparing the 3D geometries acquired with the two scanners. The two geometries are aligned into a common reference frame by a first rough pairwise alignment followed by a global registration. The model obtained by using the stationary scanner is used as the reference. The distribution of the deviation values is characterized by a mean value $\mu = 1.24$ mm, an absolute mean value $|\mu| = 1.36$ mm, and a standard deviation value $\sigma = 1.40$ mm. Positive deviation values mean that test points lay outside the

Fig. 7 Acquisition of the plaster hand: (a) setup of the stationary scanner, (b) 3D mesh obtained with the stationary scanner, and (c) with the developed hand-held scanner

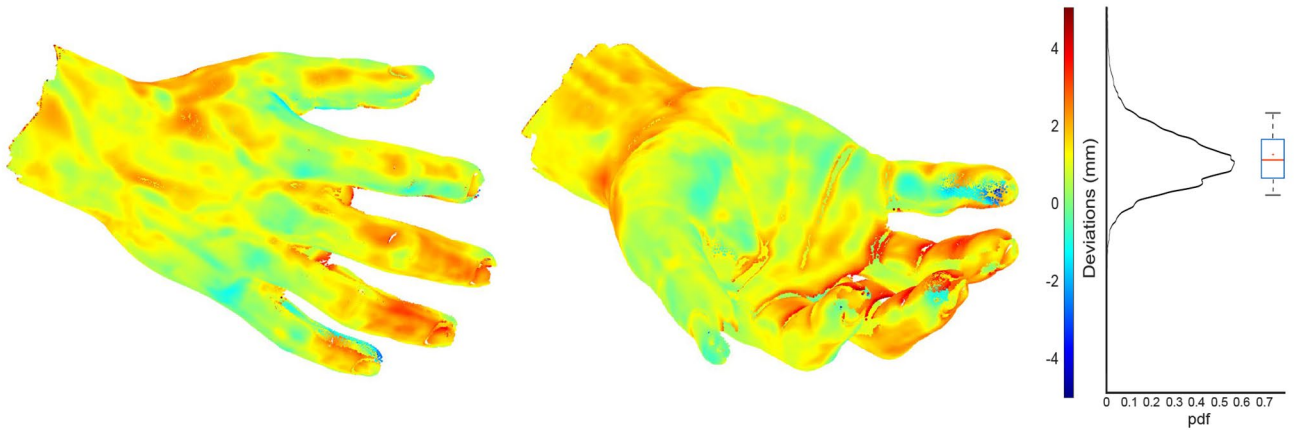

Fig. 8 Two views of the 3D comparison between the plaster hand models obtained by using the developed scanner and the reference stationary scanner. The histogram of the deviation values is also reported with the associated probability distribution function

reference mesh, while negative deviation values mean that the points are inside the mesh.

The 2D deviations in correspondence of three anatomical significant sections of the models were computed to better compare the two scanning results. The sections have been obtained by using planes perpendicular to the hand axis, which has been estimated by selecting the principal axis of inertia of the point cloud. Figure 9 reports the results obtained in correspondence of a wrist section (Fig. 9(a)), a palm section (Fig. 9(b)), and a fingers section (Fig. 9(c)). Figure 9(d) shows the three corresponding histograms for the 2D deviations on the three section planes. As can be seen in Fig. 9(a), all the points along the wrist present positive 2D deviation values ($\mu = 1.44$ mm, $|\mu| = 1.44$ mm, $\sigma = 0.35$ mm). The palm (Fig. 9(b)) presents lower deviation values ($\mu = 0.60$ mm, $|\mu| = 0.64$, $\sigma = 0.44$ mm). It is worth noting that the palm width almost coincides between the two models, while the most significant differences emerge in the knuckles area. This can be explained by the fact that the stationary scanner can capture highly detailed geometries, while the developed scanner tends to produce smoother scans due to the lower resolution. However, the 2D deviations in terms of hand measurements are limited.

The highest differences can be observed in the fingers' area (Fig. 9(c), $\mu = 1.32$ mm, $|\mu| = 1.35$ mm, $\sigma = 0.85$ mm). However, only a limited number of points have a value higher than 2 mm. It is worth noting that the finger region is the most challenging region for the acquisition, because of self-undercuts, fast slope variation of the surface, and a greater tendency to involuntary movements of the fingers themselves.

The comparison between the two full 360° acquisitions, however, could be also influenced by the alignment process between the different frames captured by each scanner and by the relative orientation between the scanner and the target surface. For this reason, a comparison between two

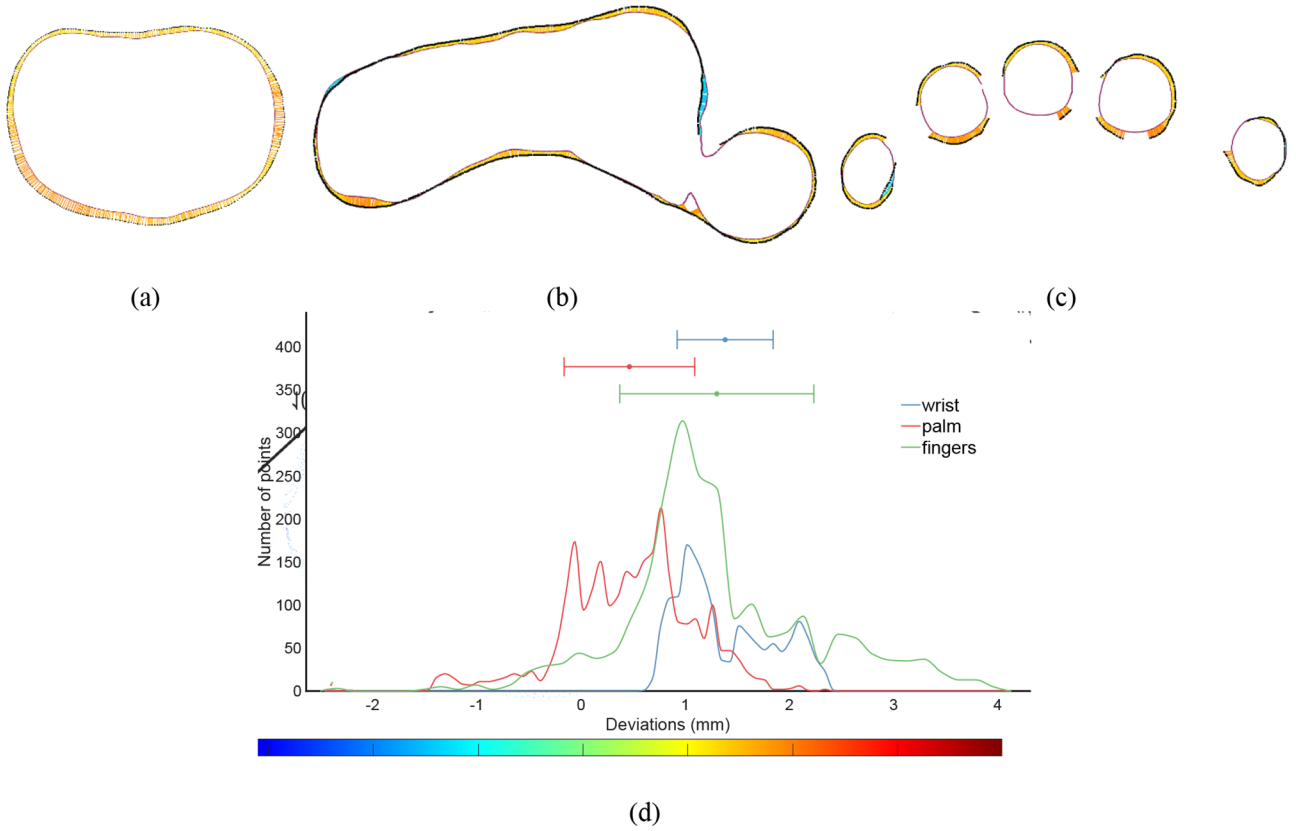

Fig. 9 2D comparison between the 3D acquisitions of the two devices for the plaster hand in correspondence of anatomical significant sections of the models: (a) wrist, (b) palm, (c) fingers. Corresponding deviations histograms (d)

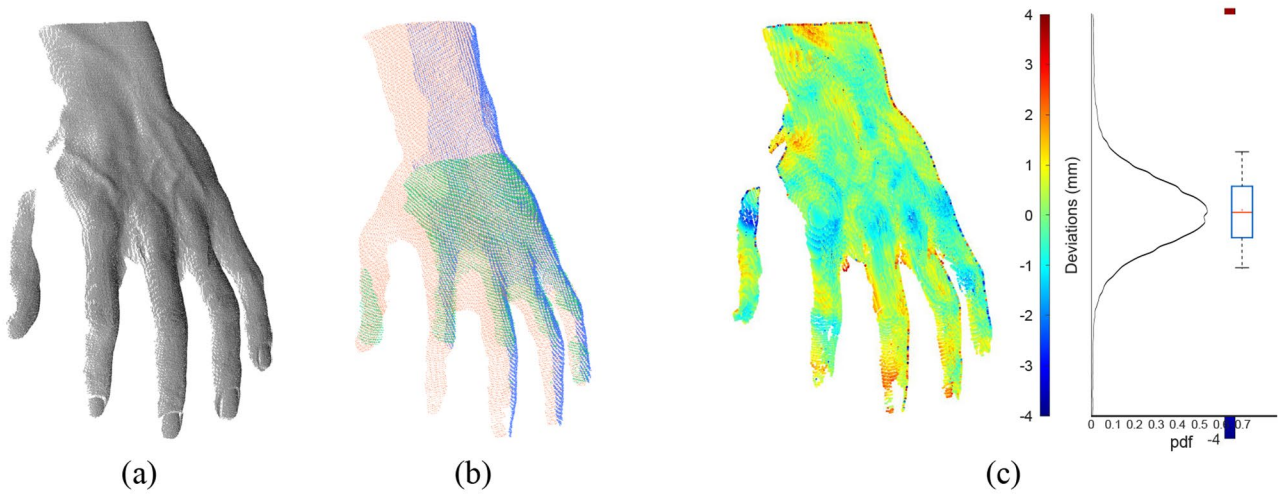

Fig. 10 3D acquisitions of the plaster hand with the stationary scanner (a) and the developed depth-camera-based scanner (b) obtained by considering a single pose of the two scanners. The 3D deviation map between the two scans is also reported along with the relative histogram (c)

single-frame acquisitions has been also carried out. Figure 10(a) and (b) show the resulting point clouds obtained by the stationary scanner and the hand-held scanner, respectively. In Fig. 10(b), the three aligned acquisitions, obtained by the three different sensors, are represented with different colors. The comparison between Fig. 10(a) and Fig. 10(b) highlights that the integration of three sensors in the hand-held scanner allowed to obtain a larger field of view compared to the stationary scanner. Figure 10(c) reports the 3D deviation map between the two models and the histogram

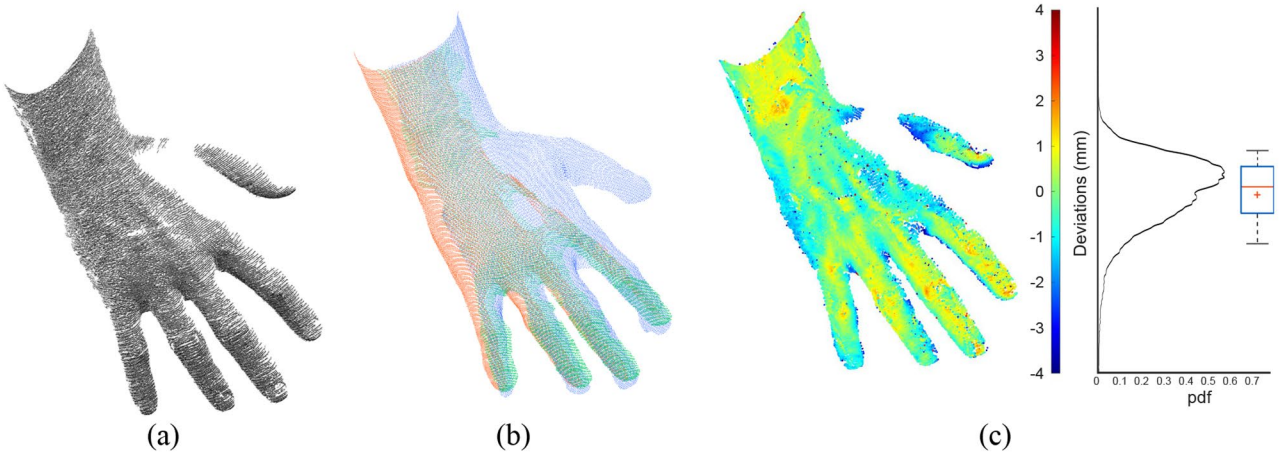

Fig. 11 3D acquisition of an actual human hand with the stationary scanner (a) and the developed depth-camera-based scanner (b) obtained by considering a single pose of the two scanners. The 3D deviation map between the two scans is also reported along with the relative histogram (c)

of the deviation distribution. It emerges that the deviation values are very limited ($\mu = 0.10$ mm, $|\mu| = 0.92$ mm, $\sigma = 1.70$ mm). The developed depth camera-based scanner demonstrates to capture a larger region of the target object with a single scanner pose but with a lower detail level, due to the lower spatial resolution than the stationary scanner. The simultaneous capturing of three registered point clouds for each pose, indeed, reduces the total number of required viewpoints. This aspect is crucial when the 3D acquisition process concerns human subjects and even more for patients with upper limb mobility disorders.

3.2 Comparison with a real hand

The developed system has been finally tested in the 3D acquisition of an actual human hand. In this case, the hand has been acquired with a single pose by each scanner given the difficulty of completing a 360° acquisition of a real arm with the stationary scanner. Moving this scanner around the arm, indeed, is complex due to its cumbersomeness and the long scanning time not compatible with the patient's comfort. Figure 11(a) and (b) show the resulting point clouds obtained by the stationary scanner and the hand-held scanner, respectively. Figure 11(c) reports the 3D deviation map between the two models and the histogram of the deviation distribution. Similarly to what was observed for the 3D acquisition of the plaster hand, deviation values are very limited (μ = -0.07 mm, $|\mu|$ = 0.70 mm, $\sigma = 1.11$ mm), and the depth-camera-based scanner can acquire a larger region of the surface thanks to the triplet of registered point clouds. Figure 11(a) also highlights that the stationary scanner, due to the longer acquisition times, has major problems in acquiring a slightly moving target, as a hand. Indeed, the resulting point cloud is noisier (especially on the fingers' area) and some lines are completely missing from the acquisition. This can be mainly ascribed to small involuntary movements of the hand and fingers during the sequential projection of the fringe patterns. On the other hand, the depth-camera-based scanner is less affected by this issue due to the high frame rate of the adopted sensors.

4 Conclusion

In this paper, the development of a low-cost, hand-held 3D scanner for the acquisition of upper limb anatomies has been presented. The scanner integrates three D415 Intel® RealSense™ depth cameras assembled on a circular frame to widen the field of view of each scanner pose. A pedal switch, ergonomic handles, and cable management were designed to ensure a fast and comfortable use of the scanner even by unskilled personnel. Moreover, an ad-hoc calibration process was defined and tested to allow for the automatic registration of the point clouds acquired by the three sensors. The performances of the depth-camera-based scanner were compared with those of a high-end structured light stationary scanner. Several tests were carried out on both a plaster hand and a real human hand, to also assess the effect of involuntary patient movement. The tests demonstrated that, as expected, the stationary scanner provides a higher detail level and more accurate acquisitions in the case of stationary objects. On the other hand, in the case of human anatomies subject to small movements, the hand-held scanner was demonstrated to provide lower noise and better acquisition results, especially in terms of measurement times since a whole 360° acquisition of a human arm requires about 30 s. The proposed scanning architecture overcomes typical limitations in the use of stationary scanners for the real-time scanning of actual patients, which are represented by the difficulties in moving the scanner around

the target surface and the high scanning times. Further research efforts should be directed toward the development of fully automated procedures for data post-processing, which would allow to drastically reduce the point clouds registration time and, at the same time, improve the repeatability and the objectivity of the scanning outcomes.

Acknowledgements This project has received funding from the European Union's Horizon 2020 research and innovation programme under grant agreement No 856998.

Funding Open access funding provided by Università di Pisa within the CRUI-CARE Agreement.
Open access funding provided by Università di Pisa within the CRUI-CARE Agreement.

References

1. Haleem, A., Javaid, M.: 3D scanning applications in medical field: a literature-based review. Clin. Epidemiol. Glob. **7**, 199–210 (2019)
2. Friel, K., Ajimaporn, P., Straub, J., Kerlin, S.: The Use of 3D Scanning for Sporting Applications. Three-Dimensional Imaging, Visualization, and Display 2015 9495, (2015)
3. Dianat, I., Molenbroek, J., Castellucci, H.I.: A review of the methodology and applications of anthropometry in ergonomics and product design. Ergonomics. **61**, 1696–1720 (2018)
4. D'Apuzzo, N.: 3D body scanning technology for fashion and apparel industry - art. no. 64910O. P Soc Photo-Opt Ins 6491, O4910-O4910(2007)
5. Xia, S.B., Guo, S.M., Li, J.Y., Istook, C.: Comparison of different body measurement techniques: 3D stationary scanner, 3D handheld scanner, and tape measurement. J. Text. Inst. **110**, 1103–1113 (2019)
6. Bartol, K., Bojanic, D., Petkovic, T., Pribanic, T.: A review of body measurement using 3D scanning. Ieee Access. **9**, 67281–67301 (2021)
7. Baronio, G., Harran, S., Signoroni, A.: A Critical Analysis of a Hand Orthosis Reverse Engineering and 3D Printing Process. Appl Bionics Biomech (2016) (2016)
8. Buonamici, F., Furferi, R., Governi, L., Lazzeri, S., McGreevy, K.S., Servi, M., Talanti, E., Uccheddu, F., Volpe, Y.: A practical methodology for computer-aided design of custom 3D printable casts for wrist fractures. Visual Comput. **36**, 375–390 (2020)
9. Barrios-Muriel, J., Romero-Sanchez, F., Alonso-Sanchez, F.J., Rodriguez Salgado, D.: Advances in Orthotic and Prosthetic Manufacturing: A Technology Review. Materials **13**, (2020)
10. Chu, C.H., Wang, I.J., Sun, J.R., Liu, C.H.: Customized designs of short thumb orthoses using 3D hand parametric models.Assist Technol (2020)
11. Volonghi, P., Baronio, G., Signoroni, A.: 3D scanning and geometry processing techniques for customised hand orthotics: an experimental assessment. Virtual Phys. Prototy. **13**, 105–116 (2018)
12. Paterson, A.M., Bibb, R., Campbell, R.I., Bingham, G.: Comparing additive manufacturing technologies for customised wrist splints. Rapid Prototyp. J. **21**, 230–243 (2015)
13. Barone, S., Neri, P., Paoli, A., Razionale, A.V., Tamburrino, F.: Development of a DLP 3D printer for orthodontic applications. Procedia Manuf. **38**, 1017–1025 (2019)
14. Paoli, A., Neri, P., Razionale, A.V., Tamburrino, F., Barone, S.: Sensor Architectures and Technologies for Upper Limb 3D Surface Reconstruction: A Review. Sensors-Basel **20**, (2020)
15. Chiu, C.Y., Thelwell, M., Senior, T., Choppin, S., Hart, J., Wheat, J.: Comparison of depth cameras for three-dimensional reconstruction in medicine. P I Mech Eng H. **233**, 938–947 (2019)
16. Li, J., Tanaka, H.: Feasibility study applying a parametric model as the design generator for 3D–printed orthosis for fracture immobilization. 3D Print. Med. **4**, 1 (2018)
17. Carfagni, M., Furferi, R., Governi, L., Servi, M., Uccheddu, F., Volpe, Y., Mcgreevy, K.: Fast and low cost acquisition and reconstruction system for human hand-wrist-arm anatomy. Procedia Manuf. **11**, 1600–1608 (2017)
18. Vitali, A., Togni, G., Regazzoni, D., Rizzi, C., Molinero, G.: A virtual environment to evaluate the arm volume for lymphedema affected patients. Comput Meth Prog Bio **198**, (2021)
19. Buonamici, F., Carfagni, M., Puggelli, L., Servi, M., Volpe, Y.: A fast and Reliable Optical 3D scanning system for human arm. In: Roucoules, L., Paredes, M., Eynard, B., Morer Camo, P., Rizzi, C. (eds.) Advances on Mechanics, Design Engineering and Manufacturing III, pp. 268–273. Springer International Publishing, Cham (2021)
20. Wang, Z.Z., Zhang, C.S.: Three-Dimensional Hand Reconstruction by single-shot structured Light Line Pattern. Ieee Access. **6**, 59881–59890 (2018)
21. Intel® RealSense™ Depth Camera D: 415, https://www.intelrealsense.com/depth-camera-d415/, last accessed 15 June 2022
22. Carfagni, M., Furferi, R., Governi, L., Santarelli, C., Servi, M., Uccheddu, F., Volpe, Y.: Metrological and Critical Characterization of the Intel D 415 Stereo Depth Camera. Sensors-Basel **19**, (2019)
23. Leap, M., Controller: www.ultraleap.com/product/leap-motion-controller/, last accessed 15 June 2022
24. Chen, C., Yang, B.S., Song, S., Tian, M., Li, J.P., Dai, W.X., Fang, L.N.: Calibrate Multiple Consumer RGB-D Cameras for Low-Cost and Efficient 3D Indoor Mapping. Remote Sens-Basel **10**, (2018)
25. Zhu, H., Guo, B., Zou, K., Li, Y.F., Yuen, K.V., Mihaylova, L., Leung, H.: A Review of Point Set Registration: From Pairwise Registration to Groupwise Registration. Sensors-Basel **19**, (2019)
26. Barone, S., Paoli, A., Razionale, A.V.: A coded structured light system based on primary color stripe projection and monochrome imaging. Sensors-Basel. **13**, 13802–13819 (2013)
27. Grazioso, S., Selvaggio, M., Di Gironimo, G.: Design and development of a novel body scanning system for healthcare applications. Int. J. Interact. Des. M. **12**, 611–620 (2018)